Hindawi Publishing Corporation
Journal of Nanomaterials
Volume 2015, Article ID 624073, 12 pages
http://dx.doi.org/10.1155/2015/624073

Research Article

Synthesis and Mechanical/Electrochemical Characterization of TiO_2 Nanotubular Structures Obtained at High Voltage

A. M. Vera-Jiménez, R. M. Melgoza-Alemán, M. G. Valladares-Cisneros, and C. Cuevas-Arteaga

Facultad de Ciencias Químicas e Ingeniería, Centro de Investigación en Ingeniería y Ciencias Aplicadas, Universidad Autónoma del Estado de Morelos, Avenida Universidad 1001, Colonia Chamilpa, 62209 Cuernavaca, MOR, Mexico

Correspondence should be addressed to C. Cuevas-Arteaga; ccuevas@uaem.mx

Received 24 August 2015; Revised 16 October 2015; Accepted 20 October 2015

Academic Editor: Yanlin Song

The synthesis of TiO_2 nanotubular arrays obtained through anodization of Ti foils in ethylene glycol (3% volume DI H_2O + 0.25 wt.% NH_4F) at high voltage is reported. The physical, chemical, electrochemical, and mechanical characterization was made to the TiO_2 nanotubular arrays. The morphological characterization showed a cylindrical geometry (112 nm inner diameter and 65 μm length), determining a rugosity factor of 1840 points. The electrochemical characterization was carried out exposing four samples: Ti, TiO_2 amorphous, and two crystalline TiO_2 nanotubular arrays (450 and 600°C) in two aqueous solutions of different pH: 1 M Na_2SO_4 and 1 M Na_2SO_4 + H_2SO_4, using the potentiodynamic polarization curves. The mechanical characterization was performed through the nanoindentation technique applying three different loads (2.5, 5.0, and 10 mN) on the amorphous and the two crystalline TiO_2 nanotubular samples, obtaining the mechanical parameters such as the hardness, the elastic module, and the maximum penetration depth. The TiO_2 nanostructured sample crystallized at 600°C had the best electrochemical stability in both media and presented an elastic modulus of 22.42 GPa when it was tested applying a load of 2.5 mN, whereas the amorphous sample presented the major hardness at the loads of 5 and 10 mN.

1. Introduction

The TiO_2 nanotubular arrays have caused great interest because of their high area/volume relationship and the new properties due to their nanometric size. The TiO_2 nanotubular films have shown to have many applications, especially due to their high oxidation potential, chemical stability, and low toxicity in animals and human beings [1]. Also, it is important to mention that titanium dioxide is a semiconductor, which acts as a good photocatalyst in presence of UV radiation [2]. TiO_2 can be found in its three allotropic forms: brookite, rutile, and anatase; the last two, but particularly the phase anatase, present a major photocatalytic activity [3, 4]. On the other hand, the nanostructured TiO_2 possesses certain desirable mechanical properties, such as high hardness and wear resistance, which becomes an attractive material for the fabrication of tools exposed in continuous motion and abrasion [5, 6]. Due to the wide spectrum of properties of TiO_2, in the last decades several authors have been working in the synthesis of nanometric titanium dioxide with different chemical approaches: sol-gel [7], hydrothermal synthesis [8], microwave irradiation [9], template synthesis [10], and anodic oxidation (also called electrochemical anodization) [11, 12]. The anodic oxidation technique is one of the most utilized techniques due to its easy application and low cost. Also, in order to control some geometric parameters such as the length and the diameter of the nanotubes, the anodization parameters (such as the applied voltage, the electrolyte concentration, and the anodization time) can be easily modified.

In 1999, Zwilling and collaborators fabricated for the first time the TiO_2 self-ordered nanostructures by anodizing Ti foils in a fluorine based electrolyte [13]. In 2001, Gong and collaborators [14] reported the fabrication of highly ordered and vertically oriented TiO_2 nanotube arrays by means of electrochemical anodization of Ti in HF aqueous electrolyte.

The TiO_2 nanoarrays consist of 1D nanocylinders with an open pore at the top and a close bottom with independent walls. Since then, there has been enormous motivation to explore different electrochemical systems in order to improve the homogeneity and the geometry of the arrays.

During the past decade, fabricated self-organized titania nanotubes have attracted wide interest due to their unique combination of nanoscale architecture and functional features [13, 15, 16]. While considerable research related to the formation of TiO_2 nanotubes is oriented to study the geometry and physical and chemical features, some other researches have been devoted to explore several applications, especially in solar cells [16–18], photoelectrolysis [19], and photocatalysis [20–22].

In many applications, TiO_2 nanotubular arrays are exposed in aqueous media with different pH; therefore their performance will depend not only on the morphological characteristics but also on their electrochemical and mechanical stability. For instance, the maximum efficiency of the photodegradation of organic compounds has been obtained in aqueous solution with a pH of 3.0. In the case of Dye-Sensitized Solar Cells (DSSCs), the mayor current density was obtained when TiO_2 nanostructured arrays were exposed to a solution with a pH of 3.0 [23]. In arthroplasty, the main aspects associated with a successful implantation are the biocompatibility and the electrochemical and mechanical stability [24]. In the last application, the electrochemical stability of the TiO_2 nanotubular arrays is especially important, considering that the pH of the body fluids lies between 5.5 and 8.0 during the time recuperation [25].

Until now, it is possible to say that many studies about TiO_2 nanostructures have been focused on determining the physical and chemical characterization together with the applications, but the mechanical characterization has been little investigated. However, shear strength and hardness can be the decisive factors in some applications, for example, in implants made with Ti alloys, which need to be coated with TiO_2 nanoporous films. The adequate joining of the implant surface and the bone tissue is crucial for the lifetime of the implant in the human body. The loss of the cohesion resulting from the friction of the implant and the human tissue can cause deterioration of the implant and an inflammatory reaction [26].

Considering those exposed above, in this paper, the synthesis of TiO_2 self-organized nanotubular arrays obtained by electrochemical anodization of titanium foils at a high voltage of 60 V using a nonaqueous electrolytic solution of ethylene glycol (3 vol.% H_2O) + 0.25 wt.% NH_4F is reported. The morphological, structural, electrochemical, and mechanical characterizations of the TiO_2 nanotubular films are also presented.

2. Materials and Methods

2.1. Synthesis of TiO_2 Nanostructures. For the formation of TiO_2 nanostructures, a classic cylindrical polytetrafluoroethylene (Teflon) cell was used, which is shown in Figure 1.

Figure 1: Teflon cell used in anodization of Ti foils.

The electrochemical cell was constituted by two electrodes, the working electrode (anode) formed by a 2 cm^2 titanium foil (the substrate) and the counter electrode (cathode) constituted by a platinum mesh. Titanium foils (99.7% purity, 0.25 mm thick, Sigma-Aldrich) were cleaned and degreased prior to the electrochemical anodization through two sonication stages of 10 minutes each, using DI water and isopropyl alcohol, respectively. The Ti foils were subsequently dried with a nitrogen stream and used immediately. No polishing or pretreatment processes were used, as recommended by Ji et al. [27]. Electrochemical anodization experiments were performed in a nonaqueous electrolytic solution of ethylene glycol (3 vol.% H_2O) + 0.25 wt.% NH_4F. The anodization process was applied for 11.5 h, keeping a constant voltage of 60 V at room temperature. After anodization, the samples were rinsed with DI water and dried in a N_2 stream.

2.2. Physical and Chemical Characterization. For morphological characterization of the TiO_2 nanotubular films, top view and cross-sectional observations were carried out with two scanning electron microscopes (SEM): LEO 1450VP and Quanta 3D FEG (Trademark FEI). Before SEM analysis, the anodized samples were previously coated with gold/palladium, which was vaporized with a Polaron SC7620 Sputter Coater device. The cross sections were obtained by bending the samples until cracking. The crystallization of TiO_2 nanotubular amorphous films was obtained introducing the samples in furnace (FELISA FE-361) heated to 450°C and 600°C. The crystalline phases of the TiO_2 nanostructure films were detected and identified on a Bruker D2 Phaser X-ray diffractometer (XRD).

2.3. Electrochemical Characterization. For the electrochemical stability, the Teflon cell described for the synthesis of the TiO_2 nanostructures was also utilized, but in this case, a three-electrode experimental setup was used. In order to make a comparison of the electrochemical performance of the nanotubular films, four samples were studied: pure titanium, an amorphous film, and the two crystallized samples. For easier identification, the four samples will be called Ti, ANT, CNT-450, and CNT-600. The working electrode was a 2 cm^2 sample, which was in contact with a copper plate as the electrical connection. The counter electrode was a platinum mesh; and the reference electrode was an

Ag/AgCl electrode. For the electrochemical characterization, two testing solutions were used: 1 M Na_2SO_4 with a pH of 6.7 and 1 M Na_2SO_4 + H_2SO_4 with a pH of 3.2. For the first case, the applied overpotential was −500 to +2000 mV, whereas for the second one it was −500 to +3000 mV. In both cases, a scan rate of 1 mV/s was applied. Prior to the measurements and in order to reach the stable state, the specimens were maintained in the solution for 30 min. potentiodynamic polarization curves were carried out using a Gill AC Instruments 1256 potentiostat/galvanostat.

2.4. Mechanical Characterization. Hardness and elastic modulus of the ANT, CNT-450, and CNT-600 samples were measured by instrumented nanoindentation technique (using a nanoindenter *Hardness Tester NHT*, CSM Instruments), with a Berkovich indenter tip. The mechanical properties were obtained from the analyses of the load-displacement data. All nanoindentation tests were performed applying loads of 2.5, 5, and 10 mN. Five tests were made for each load in different locations of the surface of the samples; then an average of the five results was determined, which is reported in this paper.

3. Results and Discussion

3.1. Physical Characterization. Figure 2 shows SEM images of the samples anodized in ethylene glycol/water (97 : 3, vol.%) with addition of 0.25 wt.% NH_4F for 11.5 h at room temperature. The diameter, wall thickness, and length of the nanotubes were obtained through the images of the top and cross section views. Figure 2(a) present a top view (open nanotubes) of a classical self-ordering TiO_2 nanotubes array as prepared, showing a uniformly distributed surface. Figure 2(b) shows the prints (with a concave shape) of the outer bottom of the inferior extreme of the nanotubes, which were resting over the barrier layer/titanium foil. Figure 2(c) shows a cross section image, from which the outer bottom surface of the nanotubes is seen in the top of the image, observing a closed packing circular-convex shape. Figure 2(d) shows the outer walls of the straight nanotubes, which show smooth rings around them. Figure 2(e) shows a cross section view of the nanotubular film, showing the thickness of the nanotubular film. Figure 2(f) shows a front view of the outer bottom surface of the nanotube array. From these images, it was possible to determine the average inner diameter of the TiO_2 nanotubes, which was 112 nm, and the wall thickness of 44 nm, as well as the length of the self-organized TiO_2 nanotubes, which was 65 μm. Also, it was observed that the nanotubes have a cylindrical geometry.

As it was said before, the TiO_2 nanotubular arrays can be used in DSSCs, for which it has been determined that the solar conversion efficiency can be strongly enhanced when nanotubes possess rings around the outer walls (bamboo-type) [28]. From Figures 2(b) and 2(c), it is possible to observe the circular shape of the nanotubes, being in concordance with the topography of the top view, although some nanotubes seem a little bit deformed due to the presence of some other nanotubes around them, which can be an indicative of the conformability reported by other authors [29]. Also, the verticality of the nanotubes with respect to the substrate shown in Figures 2(c) and 2(d) is extraordinary, as well as the length, which is good enough in order to obtain a large surface area needed in almost all the possible applications.

Figure 3(a) shows the current-time behavior obtained during the 11.5 h of the anodization process in the formation of the TiO_2 nanotubular film, whereas Figure 3(b) shows a detail of the current transient during the first 10 min of anodization. From Figure 3(b), the existence of three stages (I, II, and III) is observed. The decay of the current is the typical behavior obtained during the self-organizing growth of Al_2O_3 and TiO_2 nanotubular films [30]. During stage I, which lasts approximately 60 s, the current response is the highest and keeps constant, as an indicative of the polarization resistance of pure titanium when exposed to the electrolyte and a constant voltage is applied. The titanium oxide layer is formed when cations Ti^{+4} (produced from the oxidation of Ti together with the corresponding electrons) are diffusing outward from the metallic surface and anions O^{-2} (from the water content) are diffusing inward into the metallic surface. During the initial electrochemical and chemical processes, a compact, protective, and adherent barrier oxide layer is formed, ejecting a great amount of electrons, which generates the highest electronic current response. At this time the pure titanium is very active in presence of the electrolyte containing oxygen and ions flour as powerful oxidants. During stage II, the oxidation of titanium and the interchange of ions Ti^{+4} and O^{-2} continue together with the diffusion of ions flour through the titanium oxide layer; therefore this layer becomes highly contaminated of a great amount of ions flour, so the current decays from 35 mA to 5 mA during the first 3 minutes. With the inward diffusion of flour, the initially planar TiO_2 layer starts to crack in a localized way, which extend along the entire oxide surface, starting the formation of the nanotubes, which has been reported widely from several scientific approaches [16, 31–33]. During stage III, the current keeps in its lowest values, and the oxidation and dissolution processes are present at the same time until the optimal formation of the nanotubular film is completed.

The roughness factor (RF) has been calculated from some parameters provided from the physical observations and the geometry calculations (see Figure 4). RF is a parameter representing the total area of the nanotubular film, which is crucial in technological applications such as sensors, photocatalysis, and photovoltaic solar cells. For instance, in dye-sensitized solar cells, the amount of sunlight collected by the monolayer surface is directly related to the *roughness factor* of the nanostructured film. Given the tube length L, the inner diameter D, and the wall thickness W, the geometric roughness factor is calculated with the next mathematical relationship [33, 34]:

$$\mathrm{RF} = 1 + \left[\frac{4\pi L\,(D + W)}{\sqrt{3}\,(D + 2W)^2} \right]. \quad (1)$$

Taking into account the geometry parameters of the TiO_2 nanotubular arrays obtained from SEM, a roughness factor was determined of 1840 points. Table 1 presents a comparative analysis of RF of TiO_2 nanotubular arrays obtained in electrochemical systems similar to that presented in this paper.

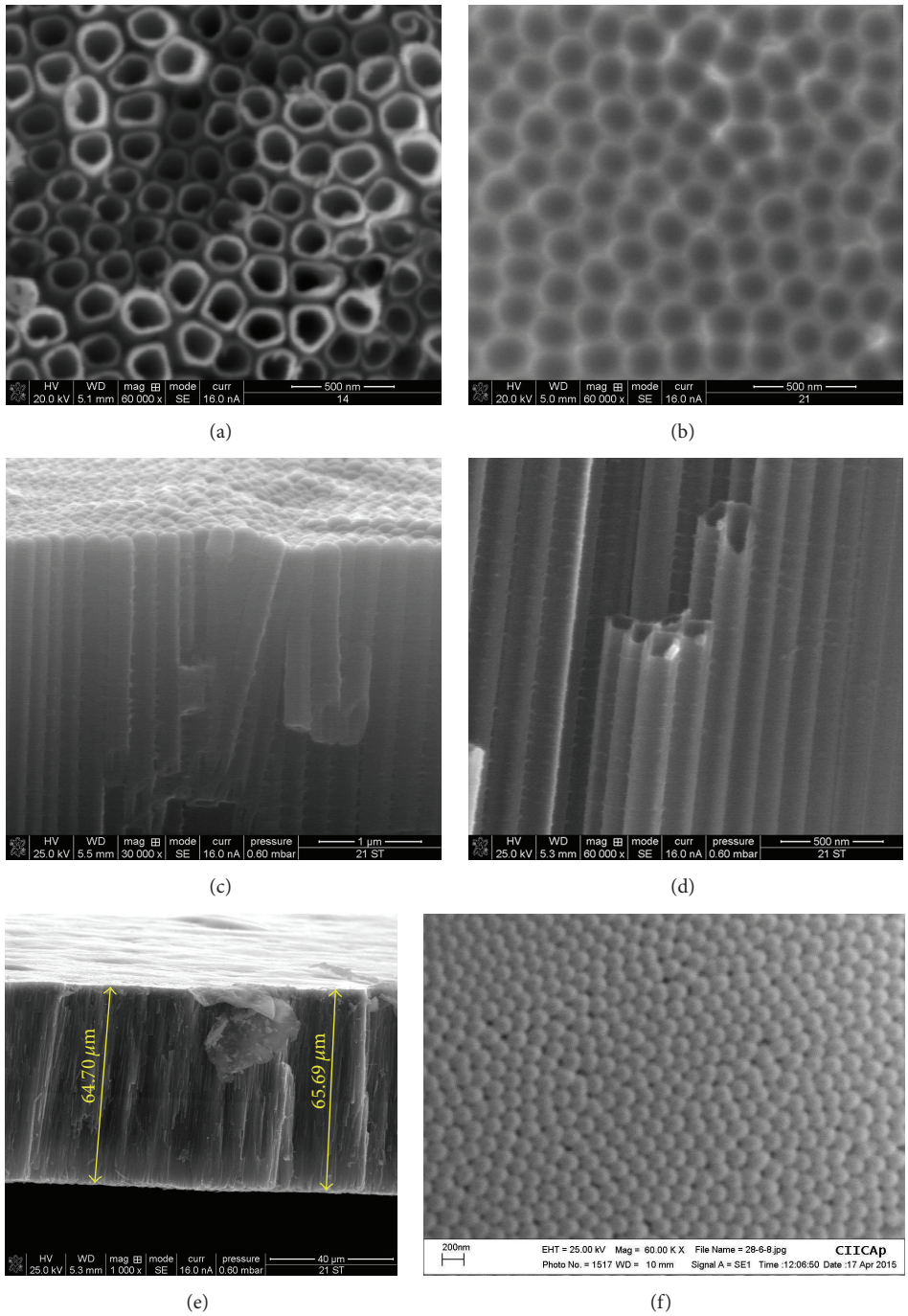

Figure 2: (a) Top view (open nanotubes) of a classical self-ordering of TiO_2 nanotube arrays. (b) Prints of the outer bottom with a concave shape. (c) Bottom/cross section view of the closed packing convex nanotubular film. (d) Outer walls of the nanotubes. (e) Cross section view of the nanotubular array. (f) Front view of the closed outer bottom surface of the nanotube array.

It can be appreciated that the RF obtained in our research is superior in 1708 points and 1545 points with respect to that obtained by Dumitriu et al.'s research group [35] and Solís de la Fuente et al. [36], respectively.

In order to clarify the impact of the parameter RF, and considering the geometry of the nanotubes, the superficial area of $1\,\mu m^2$ of the TiO_2 nanostructures was calculated theoretically and geometrically. Such calculation clearly showed that just $1\,\mu m^2$ of the TiO_2 nanostructured array becomes $573\,\mu m^2$. Figure 4 shows schematically the sequence of that calculation.

Dumitriu et al. [35] carried out their research utilizing a solution of ethylene glycol-H_2O (98 : 2 vol.%) + 0.5 wt.% NH_4F, anodizing Ti mirror-like foils at a voltage of 50 V,

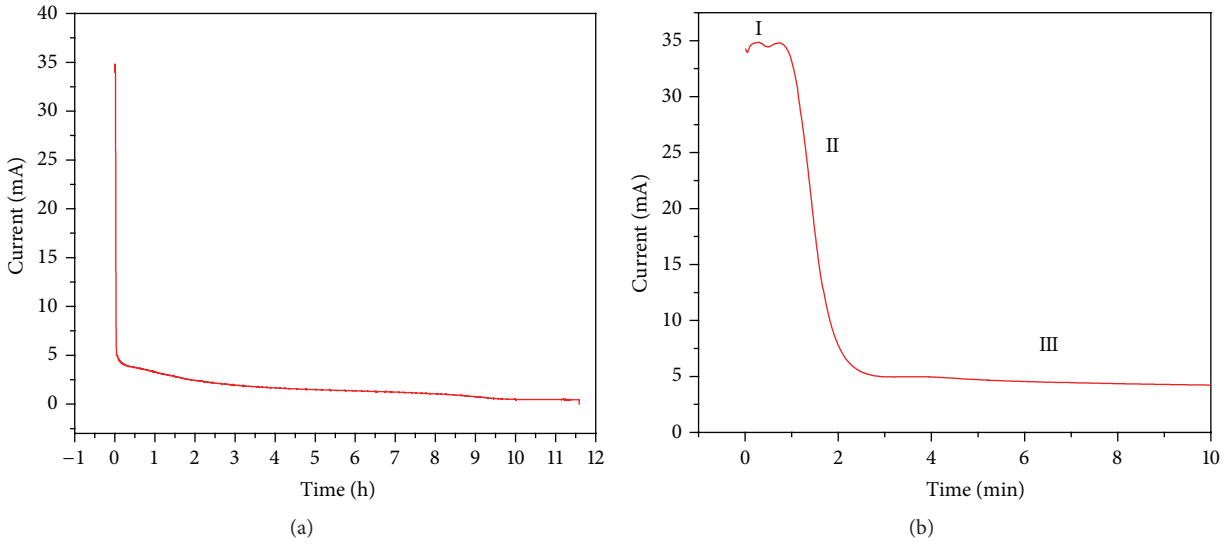

FIGURE 3: (a) Current transient recorded during the 11.5 h of the anodization process. (b) A detail of the current transient during the first 10 min of the anodization process.

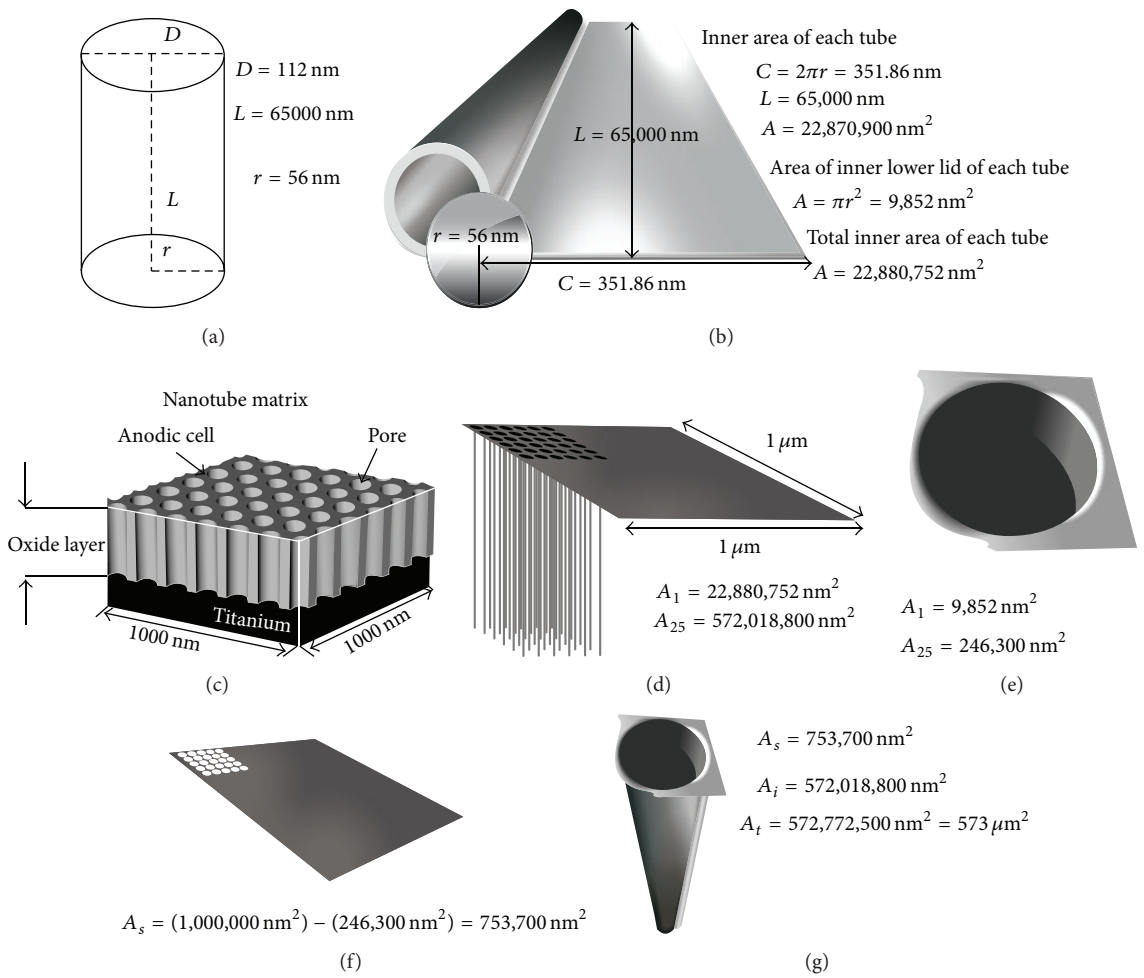

FIGURE 4: Calculation of the superficial area: (a) dimensions of the nanotube. (b) Total inner area of each nanotube. (c) Nanotubes present in 1 μm^2. (d) Inner area of 25 tubes. (e) Area of 25 upper holes. (f) Total superficial area free of holes. (g) Sum of all the areas (inner and superficial).

Table 1: Comparison of RF obtained from other references [35, 36].

Authors	Inner diameter D (nm)	Length L (μm)	Wall thickness W (nm)	RF
(1) The present work	112	65	44	**1840**
(2) Dumitriu et al. [35]	100	2.65	13	132.2
(3) Solís de la Fuente et al. [36]	100	8	30	295

which was applied increasing from 0 to 50 V with a scan rate of 2 V/10 s, keeping the 50 V constant during 2 h at room temperature, whereas Solís de la Fuente et al. [36] performed their experimentation using ethylene glycol-H_2O (99 : 1 vol.%) + 0.25 wt.% NH_4F, anodizing Ti foils at 50 V during 8 h. It is confirmed that the lower amount of water used by Dumitriu et al. with the inherent decrease of oxygen as a powerful oxidant and the minor anodization time reduce the formation of titanium oxide; therefore the thickness of the nanostructured film is smaller. On the other hand, the applied voltage by Dumitriu was 10 V lower than that applied in the present research. This is an important feature in the determination of the nanotube lengths. Wan et al. [29] reported different anodizations of Ti foils exposed in ethylene glycol-H_2O (98 : 2 vol.%) + 0.3 wt.% NH_4F during 18 h, applying several voltages: 30 V, 40 V, 50 V, 60 V and 70 V. They found that the nanotubes length were increasing when applying the voltages from 30 V to 60 V, nevertheless when they applied 70 V, the nanotubes length suffered a decrease with respect to the nanotubes length obtained at 60 V. Also, the growth rate when the applied voltage increased from 50 V to 60 V was two and a half times more than that when the voltages increased from 30 to 40 V and from 40 to 50 V. This behavior seems to indicate that 60 V is a critical condition in the growth of nanotubes under the exposure of Ti foils in the solution of ethylene glycol-H_2O-NH_4F, since the electric field and therefore the electromotive force seem to improve the oxidation reactions to form a dense oxide layer. From the above statement, and considering that the anodization time was just 2 h, it seems to be understandable why the nanotubes length obtained by Dumitriu et al. resulted in being very short. With respect to the Solís de la Fuente et al. results, it is expected that, with an even smaller amount of water and a smaller concentration of NH_4F, the nanotubes length would be smaller than that reported in this paper; nevertheless, the anodization time, which was 8 h, enhanced the nanotubes length, as has been reported by several authors [25, 28, 30, 32].

3.2. Chemical and Structural Characterization. Figure 5 shows the XRD patterns of the ANT and the two crystallized TiO_2 nanotubes samples. The results showed that the crystalline phases of the samples varied according to the temperatures (450°C and 600°C). As expected, only one pattern (a) showed peaks of Ti substrate in 2θ = 39°, 40.5°, 53.8°, 63°, and 70.9°. In addition, an intense background noise was observed, indicating that the dominant phase of the noncrystallized TiO_2 nanotubes arrays was amorphous [37]. (b) and (c) patterns showed the crystalline phases of the nanotubes crystallized for 2 h at 450°C and 600°C, respectively. Anatase and rutile phases appeared once the

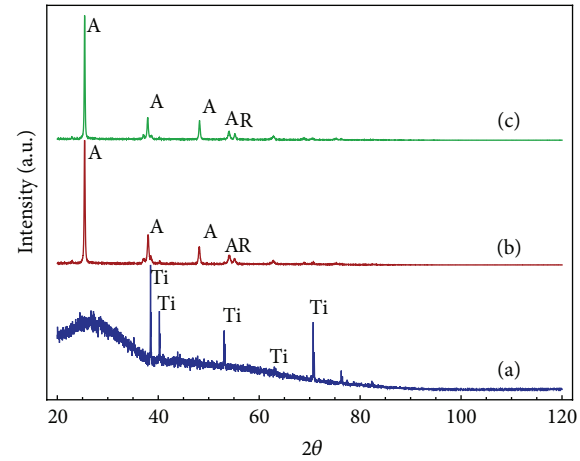

Figure 5: XRD patterns of the studied TiO_2 nanotubes samples: (a) amorphous; (b) crystallized at 450°C; (c) crystallized 600°C.

amorphous samples were crystallized at both temperatures. (b) and (c) patterns show the presence of anatase structures in 2θ = 25.2°, 37.8°, 48°, and 53.8° (PDF # 21-1272, JCPDS), whereas rutile was detected in small proportion and coexisting with anatase in 2θ = 54°, and in independent form in 2θ = 55° (PDF # 21-1272, JCPDS). Based on the fact that rutile phase is more stable than the anatase phase, it can be inferred that the transformation phases from anatase to rutile are produced at higher crystallization temperatures. However, there is also evidence that, at temperatures higher than 600°C, nanotube structures can be collapsed [38].

In (b) and (c) patterns of the crystalline phases of the nanotubes, it must be noticed that the intensity of the peaks of Ti corresponding to 39°, 40.5°, 53.8°, 63°, and 70.9° becomes less intense, which indicates that the remaining Ti substrate is oxidized by O_2 during the exposition to high temperatures.

3.3. Electrochemical Characterization. In order to determine the electrochemical stability of crystalline and amorphous Ti/TiO_2 nanostructured films, the electrochemical potentiodynamic polarization technique was applied. The importance of the electrochemical stability of the TiO_2 nanotubular films is due to the possible application in liquid media, which could degrade the film from an electrochemical point of view. For instance, the TiO_2 nanostructures could be used in dental prosthesis exposed in human saliva, which has a pH of 6.7–6.8. The test solutions for determining the electrochemical stability were two: an aqueous solution 1 M Na_2SO_4 (pH = 6.7) [39–41] and the aqueous solution 1 M Na_2SO_4 + H_2SO_4 (pH = 3.2).

Table 2: Electrochemical parameters of the potentiodynamic polarization curves.

Sample	Parameters of the curves with 1 M Na_2SO_4 solution			Parameters of the curves with 1 M Na_2SO_4 + H_2SO_4 solution		
	I_{corr} (mA/cm^2)	E_{corr} (mV)	R_p (Ω cm^2)	I_{corr} (mA/cm^2)	E_{corr} (mV)	R_p (Ω cm^2)
Pure Ti	2.59×10^{-5}	−182	8.7×10^5	5.4×10^{-5}	−44	7.1×10^5
Amorphous TiO_2	2.10×10^{-3}	−618	1.1×10^4	1.02×10^{-3}	−318	2.3×10^4
TiO_2 crystallized at 450°C	2.54×10^{-4}	−396	1.1×10^5	2.5×10^{-3}	−246	7.4×10^3
TiO_2 crystallized at 600°C	8.6×10^{-6}	−235	1.9×10^6	1.1×10^{-4}	−150	2.4×10^5

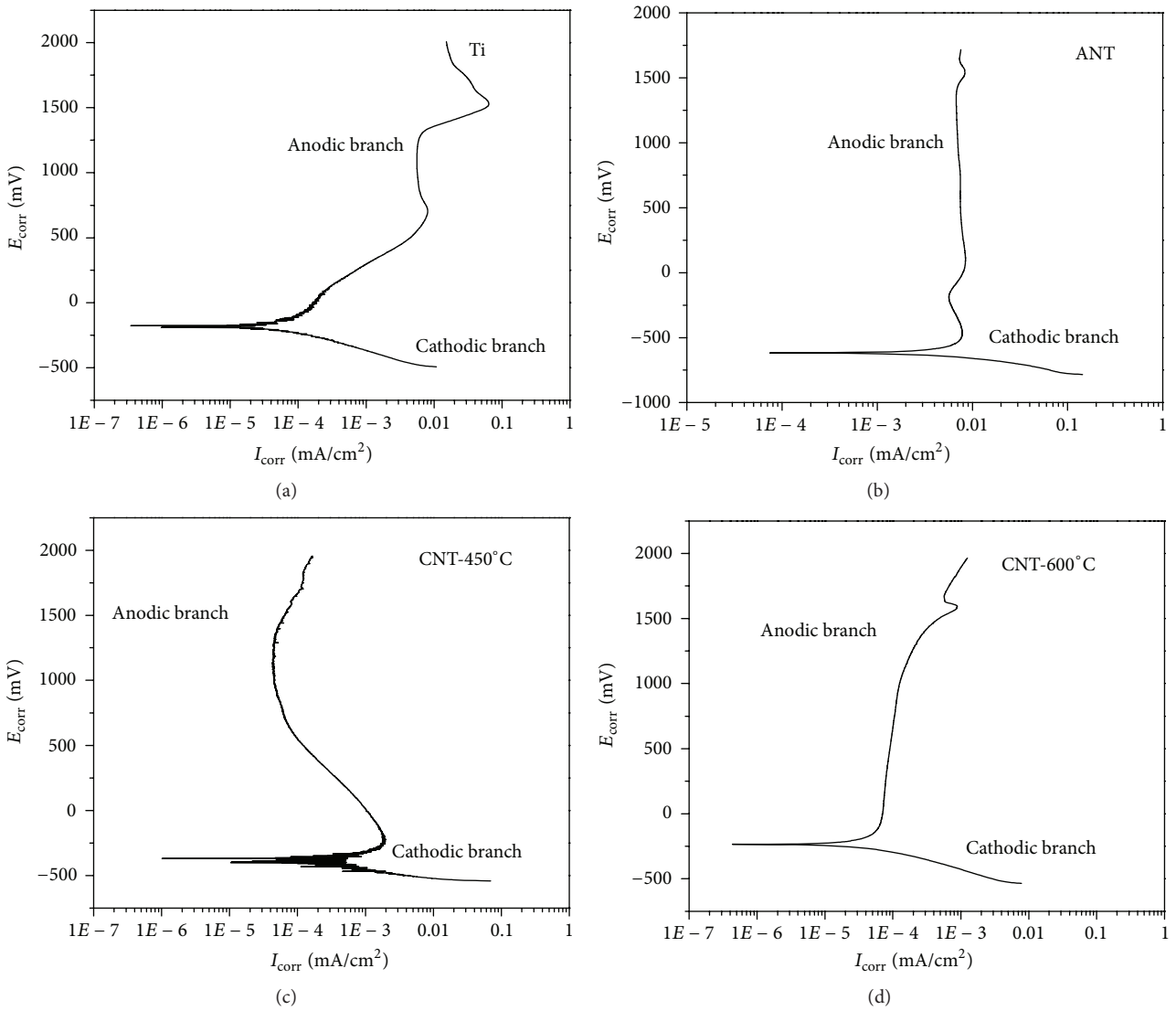

Figure 6: Potentiodynamic polarization curves of the four different samples obtained in the aqueous solution 1 M Na_2SO_4 (pH = 6.7) at room temperature.

Figure 6 presents the potentiodynamic polarization curves (PC) of the four studied samples. The Tafel extrapolation method was applied in order to determine the current density corrosion rate in stable state (I_{corr}) and the corrosion potential (E_{corr}), whereas the polarization resistance (R_p) was calculated theoretically (see Table 2). Also, when the anodic applied potential is big enough like in this case (+2000 and +3000 mV), it is possible to obtain certain information about the corrosion mechanism. For comparison purposes, the interpretation and analysis of the corrosion behavior of pure Ti will be presented before the other three samples. Taking into account the corrosion potential (−182 mV), Ti is the noblest material (less active); nevertheless, the current density is major than that presented

for CNT-600. From the anodic branch, it is observed that Ti sample behaved always actively until 650 mV, increasing its current density at 0.009 mA/cm^2; at this moment a thick, compact, and protective planar oxide layer has been formed. Then a passivation was seen, decreasing the current density at 0.005 mA/cm^2 at a potential of 1325 mV. Afterward, and due to the presence of corrosive species, that compact layer is fluxing or dissolving, and an important increase of the current density was again observed, reaching a maximum value of 0.07 mA/cm^2. At the end of the polarization, Ti suffers a transpassivation (a second self-protection) reaching a current density of 0.018 mA/cm^2, seeming to have a tendency to keep a constant current density at the end of the test. Ti presented two events to protect itself; that is why it has been said that Ti is a very good corrosion (electrochemical) and chemical resistant material. Also, due to its good mechanical properties, it has been used in dental and bones human prosthesis [42]. However, as observed in Figure 6, the highest current densities were presented for Ti. With respect to the two crystallized samples, their current densities values were smaller than that for Ti, reaching a very low current density of 4.5×10^{-5} mA/cm^2 at a voltage of 1250 mV for CNT-450, and 7.0×10^{-5} mA/cm^2 at 250 mV for CNT-600. Some interesting features are seen for the crystallized samples. CNT-450 sample had a major I_{corr} with respect to CNT-600°C (two orders of magnitude larger) and presents an important passivation behavior reaching the smallest current density at the highest potentials, whereas at the lowest potentials (less than 520 mV) CTN-600 presented an almost constant current density with a lowest value of the current density (around 7×10^{-5} mA/cm^2). With respect to ANT sample, even though it possesses the more active corrosion potential and the highest current density, at the very beginning, it presented a passivation behavior and then a constant current density along the test, which indicates a very good electrochemical stability [43].

From the corrosion point of view, the degradation of metallic materials is expected to carry out when the oxidation and reduction reactions take part, forming metallic cations and liberating electrons (during an oxidation reaction), which will be consumed through the reduction reactions in presence of oxidant species in the electrolyte. The natural way in which the materials are protective when exposed in a corrosive media is developing a passive layer of their more stable oxide; it means that metallic materials go back to the condition in which they were initially in the earth. In the particular case of titanium, it forms TiO_2, which at room temperature is in the form of anatase. The behavior of the polarization curves of Ti and ANT is expected, since ANT behaves in some way similar to Ti when it has formed a compact, adherent, and protective layer, observing a similar behavior of both samples between 600 and 1325 mV. After 1325 mV, both materials behave very differently; the TiO_2 nanostructured amorphous sample shows its better performance. It seems to be that being the corrosion processes of a superficial phenomenon, the best electrochemical stability of ANT with respect to Ti is due to the superficial nanogeometry. ANT film has certain rugosity, which according to the calculation of the total area presented in Figure 4 is 24 : 76 approximately (void : solid TiO_2), which means that it is more difficult that the corrosive species find the solid TiO_2 in order to be dissolved, and even though there are much more superficial areas in the nanostructured material, this area is inside the nanotubes; therefore, corrosive species will have to diffuse a longer path, which makes fluxing and oxidation reactions be carried out slower. Also, it is important to remember that ANT film is above a compact, protective, and adherent barrier layer, which was formed when the anodization process began. In summary, observing the behavior of the anodic curves, the crystallized samples have the best electrochemical stability, especially the sample crystallized at the higher temperature.

Figure 7 presents the potentiodynamic polarization curves of the four different samples exposed in an aqueous solution 1 M Na_2SO_4 + H_2SO_4 (pH = 3.2) at room temperature. In general, the corrosion behavior of the potentiodynamic polarization curves obtained after the exposure in the acidic aqueous solution is very similar to that observed at the weak acidic condition, except that the CNT-450 suffers a very important increase of the current density around 1500 mV after the first passivation. Also, with respect to the ANT sample, at the very beginning of the anodic branch and after the active zone, a passivation and then an increase of the current density were seen before keeping a constant current density along the rest of the test. In general, the current density increased when the exposure was in the more acidic solution, two orders of magnitude in the case of the CNT-600 sample, and one order of magnitude in the case of the CNT-450 sample, keeping the same order of magnitude for the rest of the samples. This result shows that, from a kinetic point of view, the nanostructured crystallized samples are more susceptible to suffer electrochemical instability when exposed in a more acidic media. Nevertheless, the corrosion potential was nobler in all cases with respect to that for the less acidic solution. This finding indicates that, from the thermodynamic point of view, nanostructured TiO_2 is corrosion resistant in strong acids at room temperature.

3.4. Mechanical Characterization. Table 3 presents the average values of the hardness and the elastic modulus of the nanoindentation tests for the applied loads of 2.5, 5, and 10 mN. These results show that, for the different applied loads on the three types of samples, the penetration depth is between 0.7% and 2.5% of the nanotubular layer thickness. These percentages are lower than the 10% of the total nanostructured layer thickness (65 μm), and consequently the hardness and the elastic modulus values obtained from the nanoindentation tests are reliable; therefore, it is not necessary to consider the effect of the substrate (ISO 14577 and ASTM E2546).

The values of the elastic modules for the ANT and CNT-450 samples increased when the applied load increased from 2.5 mN to 5.0 mN; nevertheless for the higher applied load of 10 mN, the elastic modules decreased, indicating that the maximum applied load before reaching the elastic limit was 5 mN. On the contrary, in the case of the CNT-600 sample, the maximum applied load before reaching the elastic limit was 2.5 mN. Therefore, it is possible to state that the elastic

Table 3: Mean values of the hardness and the elastic modulus of the three studied samples.

Mechanical properties	Loading/unloading								
	2.5 mN	5.0 mN	10.0 mN	2.5 mN	5.0 mN	10.0 mN	2.5 mN	5.0 mN	10.0 mN
	Amorphous			Crystallized at 450°C			Crystallized at 600°C		
Hardness (MPa)	305.78	328.98	562.04	152.84	310.48	268.78	587.03	186.63	164.40
Vickers hardness (in Vickers)	28.32	30.47	52.05	14.16	28.75	24.89	54.37	17.28	15.23
Elastic module (Young's) (Gpa)	11.52	13.60	13.52	22.83	29.57	11.73	22.42	16.10	12.93
Max. penetration depth (nm)	595.80	831.66	957.16	794.65	891.53	1377.13	482.43	1139.17	1638.98

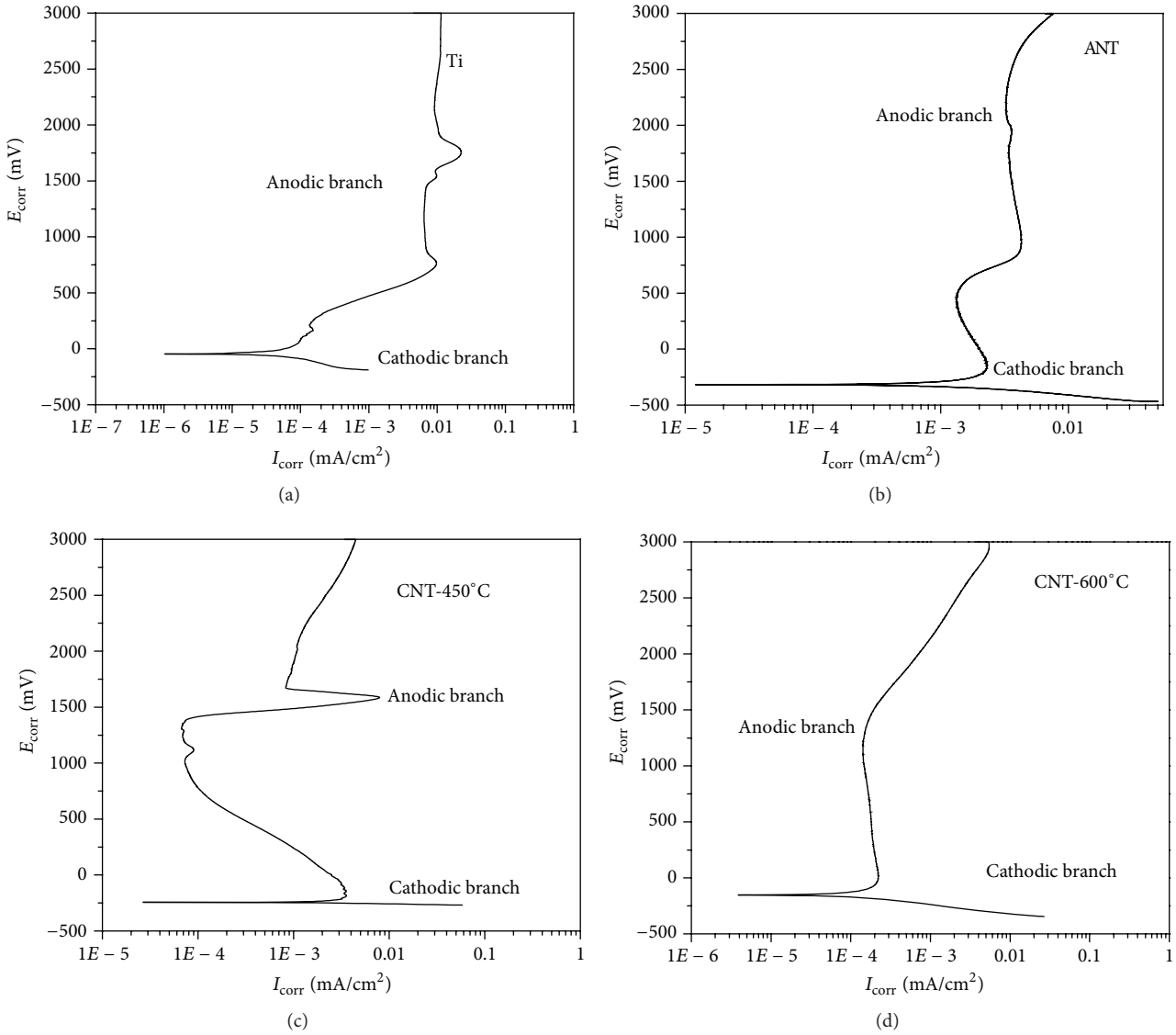

Figure 7: Potentiodynamic polarization curves of the four different samples exposed in the aqueous solution 1 M Na_2SO_4 + H_2SO_4 (pH = 3.2) at room temperature.

modules for the ANT, the CNT-450, and CNT-600 samples were 13.60 GPa, 29.57 GPa, and 22.42 GPa, respectively. These values are smaller than that reported by Jiménez-Piqué et al. and Gaillard et al. [44, 45], who obtained a value of 88 GPa for TiO_2 nanostructured samples. However, it is important to indicate that the thickness of the samples reported in both references was 500 nm, whereas the thickness of the samples reported in the present work is 65 μm. The longer length of the nanotubes reported in this work may lead to a fragile structure. On the other hand, not only an increase of the thickness samples, but also the increase in the nanoporous density can reduce the elastic modulus, as has been reported in some investigations [46–49]. It is important to allude that, for human applications, for instance, as bone substitute, the materials should have an elastic modulus similar to the bones and be porous. The porous surface of bone substitute materials is important for a good adhesion to the bone cells and for its proliferation [50]. Therefore, considering that the elastic modulus of the fresh bones (just after the skin is removed) is 21 GPa [51], it is possible to state that the TiO_2 nanotubular films crystallized at 600 could be promising candidates to be used in bones and also in dental implants.

With respect to the hardness, it has been reported that the magnitude of this parameter can suffer the Indentation Size Effect (ISE), which involves an increase of the hardness with the load, observing an increase of the residual impressions produced by the indenter tip over the nanotubular surface [52]. From a macroindentation and microindentation point of view, there are some empirical models to describe the causes originating such effect, and for determining a value of the hardness, which is independent of the applied load. The hardness independent of the load is known as *real hardness* or *hardness independent of the load*. Some reported models are Meyer's Law, Hays and Kendall approximation, Proportional Specimen Resistance (PSR) model, Modified Proportional Specimen Resistance (MPSR) model, and so forth [53, 54]. In the present work, the analysis with such models is out of the aims; nevertheless, a good explanation is that the variation of the hardness is due to the superficial rugosity and to the porosity of the TiO_2 nanostructured films.

Figure 8 shows the typical curves of load versus indentation depth for ANT, CNT-450, and CNT-600 samples subjected to a load of 5 mN. Through these nonlinear curves, the unloading data are used to determine the mechanical properties based on the indentation theory, from which the unloading curve provides the elastic recovery [55]. From such plots, it is possible to observe that the ANT and CNT-450 samples present an alike indentation depth, 831.66 and 891.53 nm respectively, the ANT sample being a little harder. Nevertheless, the major indentation depth of 1139.17 nm was for the CNT-600 sample, resulting in lower hardness. This behavior is probably due to major amount of anatase presented in this sample, so that the crystalline structure is formed with distorted octahedral with little symmetry with respect to that presented for the phase rutile. On the other hand, the lengths between Ti-Ti atoms in the phase anatase, which are 0.379 and 0.304 nm, are longer with respect to that of the phase rutile, which are 0.357 and 0.296 nm, whereas the lengths of Ti-O atoms are shorter in the phase anatase (0.1934 and 0.1980 nm) with respect to that of the phase rutile (0.1949 and 0.1980 nm) [56]. This result is in agreement with that presented by García for the microdeformation of the anatase, which resulted in 24.8% and for the rutile in 9.54% [57].

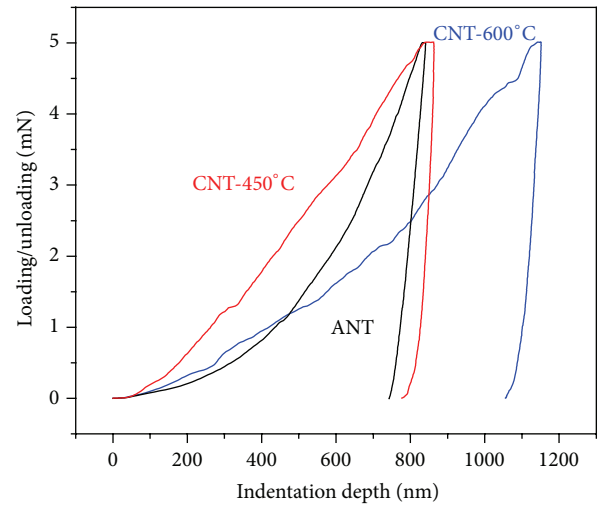

Figure 8: Loading/unloading versus indentation depth curves for an applied load of 5 mN of the three studied samples.

4. Conclusions

Highly ordered TiO_2 nanotubes arrays with a length of 65 μm were fabricated when exposing Ti foils in ethylene glycol-H_2O + 0.25 M NH_4F during 11.5 h at room temperature applying the anodization technique at a voltage of 60 volts. The TiO_2 nanotubes had an inner diameter of 112 nm and a wall thickness of 44 nm. According to the dimensions and the distribution of the TiO_2 nanotubular array, it was possible to determine that 1 μm^2 of superficial area of the nanofilm presents 573 times more area once the length of the nanotubes is considered, being the relationship of the areas of 573 μm^2/1 μm^2. The rugosity factor was calculated as 1840 points. This enormous value may be advantageous for most applications, and it is superior to those values reported elsewhere [35, 36]. According to the chemical characterization, the TiO_2 nanotubular arrays crystallized at 600°C presented a major amount of anatase, which can be beneficial for photocatalytic applications [58].

With respect to the electrochemical characterization, it was possible to determine that the TiO_2 nanotubular structure crystallized at 600°C had the best electrochemical stability in both media, obtaining the lowest current density and the noblest corrosion potential. Additionally, from the mechanical studies, this sample presented an elastic modulus of 22.42 GPa when it was tested to a load of 2.5 mN; this result is a good feature in order to be used in bone implants. Also, the ANT presented the major hardness when applying the loads of 5 and 10 mN.

Conflict of Interests

The authors declare that there is no conflict of interests regarding the publication of this paper.

Acknowledgments

This work was made with the financial support given by Conacyt-México through the project CB-2011-168772 granted to C. Cuevas-Arteaga, whereby the authors thank Conacyt for its enormous help. Also, A. M. Vera Jiménez thanks Conacyt for the scholarship received to be able to carry out her doctoral project.

References

[1] X. Cui, H.-M. Kim, M. Kawashita et al., "Preparation of bioactive titania films on titanium metal via anodic oxidation," *Dental Materials*, vol. 25, no. 1, pp. 80–86, 2009.

[2] A. Fijishima, K. Hashimoto, and T. Watanabe, *TiO_2 Photocatalysis, Fundamentals and Applications*, University of Tokyo, Tokyo, Japan, 1999.

[3] D. A. H. Hanaor and C. C. Sorrell, "Review of the anatase to rutile phase transformation," *Journal of Materials Science*, vol. 46, no. 4, pp. 855–874, 2011.

[4] K. Hashimoto, H. Irie, and A. Fujishima, "TiO_2 photocatalysis: a historical overview and future prospects," *Japanese Journal of Applied Physics*, vol. 44, no. 12, pp. 8269–8285, 2005.

[5] A. Ibrahim, R. S. Lima, C. C. Berndt, and B. R. Marple, "Fatigue and mechanical properties of nanostructured and conventional titania (TiO_2) thermal spray coatings," *Surface and Coatings Technology*, vol. 201, no. 16-17, pp. 7589–7596, 2007.

[6] R. Yılmaz, A. O. Kurt, A. Demir, and Z. Tatli, "Effects of TiO_2 on the mechanical properties of the Al_2O_3-TiO_2 plasma sprayed coating," *Journal of the European Ceramic Society*, vol. 27, no. 2-3, pp. 1319–1323, 2007.

[7] S. G. Yang, Y. Z. Liu, and C. Sun, "Preparation of anatase TiO_2/Ti nanotube-like electrodes and their high photoelectrocatalytic activity for the degradation of PCP in aqueous solution," *Applied Catalysis A: General*, vol. 301, no. 2, pp. 284–291, 2006.

[8] H.-H. Ou and S.-L. Lo, "Review of titania nanotubes synthesized via the hydrothermal treatment: fabrication, modification, and application," *Separation and Purification Technology*, vol. 58, no. 1, pp. 179–191, 2007.

[9] X. Wu, Q.-Z. Jiang, Z.-F. Ma, M. Fu, and W.-F. Shangguan, "Synthesis of titania nanotubes by microwave irradiation," *Solid State Communications*, vol. 136, no. 9-10, pp. 513–517, 2005.

[10] S.-I. Na, S.-S. Kim, W.-K. Hong et al., "Fabrication of TiO_2 nanotubes by using electrodeposited ZnO nanorod template and their application to hybrid solar cells," *Electrochimica Acta*, vol. 53, no. 5, pp. 2560–2566, 2008.

[11] G. K. Mor, O. K. Varghese, M. Paulose, and C. A. Grimes, "Transparent highly ordered TiO_2 nanotube arrays via anodization of titanium thin films," *Advanced Functional Materials*, vol. 15, no. 8, pp. 1291–1296, 2005.

[12] Z. Y. Liu, B. Pesic, K. S. Raja, R. R. Rangaraju, and M. Misra, "Hydrogen generation under sunlight by self ordered TiO_2 nanotube arrays," *International Journal of Hydrogen Energy*, vol. 34, no. 8, pp. 3250–3257, 2009.

[13] V. Zwilling, E. Darque-Ceretti, A. Boutry-Forveille, D. David, M. Y. Perrin, and M. Aucouturier, "Structure and physicochemistry of anodic oxide films on titanium and TA6V alloy," *Surface and Interface Analysis*, vol. 27, no. 7, pp. 629–637, 1999.

[14] D. Gong, C. A. Grimes, O. K. Varghese et al., "Titanium oxide nanotube arrays prepared by anodic oxidation," *Journal of Materials Research*, vol. 16, no. 12, pp. 3331–3334, 2001.

[15] J. M. Macak, H. Tsuchiya, L. Taveira, S. Aldabergerova, and P. Schmuki, "Smooth anodic TiO_2 nanotubes," *Angewandte Chemie: International Edition*, vol. 44, no. 45, pp. 7463–7465, 2005.

[16] P. Roy, S. Berger, and P. Schmuki, "TiO_2 nanotubes: synthesis and applications," *Angewandte Chemie International Edition*, vol. 50, no. 13, pp. 2904–2939, 2011.

[17] B. O'Regan and M. Grätzel, "A low-cost, high-efficiency solar cell based on dye-sensitized colloidal TiO_2 films," *Nature*, vol. 353, no. 6346, pp. 737–740, 1991.

[18] K. Shankar, G. K. Mor, H. E. Prakasam et al., "Highly-ordered TiO_2 nanotube arrays up to 220 μm in length: use in water photoelectrolysis and dye-sensitized solar cells," *Nanotechnology*, vol. 18, no. 6, Article ID 065707, 11 pages, 2007.

[19] M. Ni, M. K. H. Leung, D. Y. C. Leung, and K. Sumathy, "A review and recent developments in photocatalytic water-splitting using TiO_2 for hydrogen production," *Renewable and Sustainable Energy Reviews*, vol. 11, no. 3, pp. 401–425, 2007.

[20] A. Fujishima, X. Zhang, and D. A. Tryk, "TiO_2 photocatalysis and related surface phenomena," *Surface Science Reports*, vol. 63, no. 12, pp. 515–582, 2008.

[21] J. M. Macak, M. Zlamal, J. Krysa, and P. Schmuki, "Self-organized TiO_2 nanotube layers as highly efficient photocatalysts," *Small*, vol. 3, no. 2, pp. 300–304, 2007.

[22] Y. Lai, L. Sun, Y. Chen, H. Zhuang, C. Lin, and J. W. Chin, "Effects of the structure of TiO_2 nanotube array on Ti substrate on its photocatalytic activity," *Journal of the Electrochemical Society*, vol. 153, no. 7, pp. D123–D127, 2006.

[23] K. U. Isah, U. Ahmadu, A. Idris et al., "Betalain pigments as natural photosensitizers for dye-sensitized solar cells: the effect of dye pH on the photoelectric parameters," *Materials for Renewable and Sustainable Energy*, vol. 4, article 39, 2015.

[24] E. E. Pakos and T. Xenakis, "Titanium porous-coated implant-bone interface in total joint arthroplasty," in *Bone-Implant Interface in Orthopedic Surgery*, T. Karachalios, Ed., pp. 67–81, Springer, London, UK, 2014.

[25] W. F. Ng, K. Y. Chiu, and F. T. Cheng, "Effect of pH on the *in vitro* corrosion rate of magnesium degradable implant material," *Ciencia de los Materiales e Ingeniería C*, vol. 30, no. 6, pp. 898–903, 2010.

[26] K. J. Margevicius, T. W. Bauer, J. T. McMahon, S. A. Brown, and K. Merritt, "Isolation and characterization of debris in membranes around total joint prostheses," *The Journal of Bone and Joint Surgery—American Volume*, vol. 76, no. 11, pp. 1664–1675, 1994.

[27] Y. Ji, K.-C. Lin, H. Zheng, J.-J. Zhu, and A. C. S. Samia, "Fabrication of double-walled TiO_2 nanotubes with bamboo morphology via one-step alternating voltage anodization," *Electrochemistry Communications*, vol. 13, no. 9, pp. 1013–1015, 2011.

[28] F. Zhang, S. Chen, Y. Yin, C. Lin, and C. Xue, "Anodic formation of ordered and bamboo-type TiO_2 anotubes arrays with different electrolytes," *Journal of Alloys and Compounds*, vol. 490, no. 1-2, pp. 247–252, 2010.

[29] J. Wan, X. Yan, J. Ding, M. Wang, and K. Hu, "Self-organized highly ordered TiO_2 nanotubes in organic aqueous system," *Materials Characterization*, vol. 60, no. 12, pp. 1534–1540, 2009.

[30] W. Wei, S. Berger, C. Hauser, K. Meyer, M. Yang, and P. Schmuki, "Transition of TiO_2 nanotubes to nanopores for electrolytes with very low water contents," *Electrochemistry Communications*, vol. 12, no. 9, pp. 1184–1186, 2010.

[31] J. M. Macak, H. Hildebrand, U. Marten-Jahns, and P. Schmuki, "Mechanistic aspects and growth of large diameter self-organized TiO_2 nanotubes," *Journal of Electroanalytical Chemistry*, vol. 621, no. 2, pp. 254–266, 2008.

[32] K. S. Raja, T. Gandhi, and M. Misra, "Effect of water content of ethylene glycol as electrolyte for synthesis of ordered titania nanotubes," *Electrochemistry Communications*, vol. 9, no. 5, pp. 1069–1076, 2007.

[33] K. Shankar, G. K. Mor, H. E. Prakasam et al., "Highly-ordered TiO_2 nanotube arrays up to 220 μm in length: use in water photoelectrolysis and dye-sensitized solar cells," *Nanotechnology*, vol. 18, no. 6, Article ID 065707, 2007.

[34] K. Zhu, N. R. Neale, A. Miedaner, and A. J. Frank, "Enhanced charge-collection efficiencies and light scattering in dye-sensitized solar cells using oriented TiO_2 nanotubes arrays," *Nano Letters*, vol. 7, no. 1, pp. 69–74, 2007.

[35] C. Dumitriu, C. Pirvu, and I. Demetrescu, "The electrochemical formation and shielding mechanism of TiO_2 nanotubes in organic electrolytes with different viscosity," *Journal of the Electrochemical Society*, vol. 160, no. 2, pp. G55–G60, 2013.

[36] M. Solís de la Fuente, M. E. Rincón, M. O. Concha Guzmán, and C. Cuevas Arteaga, "Nanostructured TiO_2 arrays obtained at low and high potential," *ECS Transactions*, vol. 36, no. 1, pp. 573–580, 2011.

[37] J. A. Eastman, "Microstructural development in nanophase TiO_2 during annealing," *Journal of Applied Physics*, vol. 75, no. 2, pp. 770–779, 1994.

[38] H. Li, L. Cao, W. Liu, G. Su, and B. Dong, "Synthesis and investigation of TiO_2 nanotube arrays prepared by anodization and their photocatalytic activity," *Ceramics International*, vol. 38, no. 7, pp. 5791–5797, 2012.

[39] M. E. Rincón, C. Cuevas-Arteaga, M. S. de la Fuente, A. Estrada-Vargas, N. Casillas, and M. Bárcena-Soto, "Low-voltage anodized TiO_2 nanostructures studied by alternate current electrochemical microscopy and photoelectrochemical measurements," *Journal of Solid State Electrochemistry*, vol. 16, no. 3, pp. 977–983, 2012.

[40] M. Sánchez, C. Cuevas, and M. Rincón, "Sensors based on electrochemically deposited titania studied by AFM and EIS techniques," *ECS Transactions*, vol. 28, no. 20, pp. 9–18, 2010.

[41] Y. Lai, H. Zhuang, L. Sun, Z. Chen, and C. Lin, "Self-organized TiO_2 nanotubes in mixed organic-inorganic electrolytes and their photoelectrochemical performance," *Electrochimica Acta*, vol. 54, no. 26, pp. 6536–6542, 2009.

[42] L.-H. Li, Y.-M. Kong, H.-W. Kim et al., "Improved biological performance of Ti implants due to surface modification by micro-arc oxidation," *Biomaterials*, vol. 25, no. 14, pp. 2867–2875, 2004.

[43] A. G. Reynaud Morales, M. O. Concha Guzmán, and C. C. Arteaga, "A brief review on fabrication and applications of auto-organized TiO_2 nanotube arrays," *Corrosion Reviews*, vol. 29, no. 1-2, pp. 105–121, 2011.

[44] E. Jiménez-Piqué, L. González-García, V. J. Rico, and A. R. González-Elipe, "Nanoindentation of nanocolumnar TiO_2 thin films with single and stacked zig-zag layers," *Thin Solid Films*, vol. 550, pp. 444–449, 2014.

[45] Y. Gaillard, V. J. Rico, E. Jimenez-Pique, and A. R. González-Elipe, "Nanoindentation of TiO_2 thin films with different microstructures," *Journal of Physics D: Applied Physics*, vol. 42, no. 14, Article ID 145305, 2009.

[46] S. C. Nanjangud, R. Brezny, and D. J. Green, "Strength and Young's modulus behavior of a partially sintered porous alumina," *Journal of the American Ceramic Society*, vol. 78, no. 1, pp. 266–268, 1995.

[47] F. P. Knudsen, "Effect of porosity on Young modulus of alumina," *Journal of the American Ceramic Society*, vol. 45, pp. 94–95, 1962.

[48] R. M. Spriggs, "Expression for effect of porosity on elastic modulus of polycrystalline refractory materials, particularly aluminum oxide," *Journal of the American Ceramic Society*, vol. 44, pp. 628–629, 1961.

[49] F. P. Knudsen, "Dependence of mechanical strength of brittle polycrystalline specimens on porosity and grain size," *Journal of the American Ceramic Society*, vol. 42, no. 8, pp. 376–387, 1959.

[50] P. Soares, A. Mikowski, C. M. Lepienski et al., "Hardness and elastic modulus of TiO_2 anodic films measured by instrumented indentation," *Journal of Biomedical Materials Research. Part B Applied Biomaterials*, vol. 84, no. 2, pp. 524–530, 2008.

[51] A. Carrera, *Elasticidad y Dureza de los Huesos*, Universidad Tecnológica Equinoccial, Quito, Ecuador, 2013.

[52] J. H. Gong, J. J. Wu, and Z. D. Guan, "Description of the indentation size effect in hot-pressed silicon-nitride-based ceramics," *Journal of Materials Science Letters*, vol. 17, no. 6, pp. 473–475, 1998.

[53] C. Hays and E. G. Kendall, "An analysis of Knoop microhardness," *Metallography*, vol. 6, no. 4, pp. 275–282, 1973.

[54] H. Li and R. C. Bradt, "The microhardness indentation load/size effect in rutile and cassiterite single crystals," *Journal of Materials Science*, vol. 28, no. 4, pp. 917–926, 1993.

[55] C. Y. Tang, C. P. Tsui, D. J. Janackovic, and P. S. Uskokovic, "Nanomechanical properties evaluation of bioactive glass coatings on titanium alloy substrate," *Journal of Optoelectronics and Advanced Materials*, vol. 8, no. 3, pp. 1194–1199, 2006.

[56] U. Diebold, "The surface science of titanium dioxide," *Surface Science Reports*, vol. 48, no. 5–8, pp. 53–229, 2003.

[57] M. L. R. García, *Introducción al Método Rietveld*, Centro de Investigación en Energía, Universidad Nacional Autónoma de México, Mexico City, Mexico, 2007.

[58] R. Portela Rodríguez, *Eliminación fotocatalítica de H_2S en aire mediante TiO_2 soportado sobre sustratos transparentes en el UV-A [Tesis doctoral]*, Universidad Santiago de Compostela, 2008.